

UTILIZING TYPE IA SUPERNOVAE IN A LARGE, FAST, IMAGING SURVEY TO CONSTRAIN DARK ENERGY

ANDREW R. ZENTNER AND SUMAN BHATTACHARYA

Department of Physics & Astronomy, The University of Pittsburgh, Pittsburgh, PA 15260
The Astrophysical Journal, submitted

ABSTRACT

We study the utility of a large sample of type Ia supernovae that might be observed in an imaging survey that rapidly scans a large fraction of the sky for constraining dark energy. We consider both the information contained in the traditional luminosity distance test as well as the spread in Ia supernova fluxes at fixed redshift induced by gravitational lensing. As would be required from an imaging survey, we include a treatment of photometric redshift uncertainties in our analysis. Our primary result is that the information contained in the mean distance moduli of supernovae Ia and the dispersion of supernova Ia distance moduli complement each other, breaking a degeneracy between the present dark energy equation of state and its time variation without the need for a high-redshift ($z \gtrsim 0.8$) supernova sample. Including lensing information also allows for some internal calibration of photometric redshifts. To address photometric redshift uncertainties, we present dark energy constraints as a function of the size of an external set of spectroscopically-observed supernovae that may be used for redshift calibration, N_{spec} . Depending upon the details of potentially-available, external supernova data sets, we find that an imaging survey can constrain the dark energy equation of state at the epoch where it is best constrained w_p , with a 1σ error of $\sigma(w_p) \approx 0.03 - 0.09$. In addition, the marginal improvement in the error $\sigma(w_p)$ from an increase in the spectroscopic calibration sample drops once $N_{\text{spec}} \sim \text{a few} \times 10^3$. This result is important because it is of the order of the size of calibration samples likely to be compiled in the coming decade and because, for samples of this size, the spectroscopic and imaging surveys individually place comparable constraints on the dark energy equation of state. In all cases, it is best to calibrate photometric redshifts with a set of spectroscopically-observed supernovae with relatively more objects at high redshift ($z \gtrsim 0.5$) than the parent sample of imaging supernovae.

Subject headings:

1. INTRODUCTION

Type Ia Supernovae (SNeIa) can be used as well-calibrated standard candles with relatively little dispersion in their intrinsic luminosities (e.g., Phillips 1993; Hamuy et al. 1995; Riess et al. 1996; Prieto et al. 2006; Guy et al. 2007; Jha et al. 2007). This has allowed for recent measurements of the relation between cosmological distance and redshift, which provide the strongest contemporary evidence for an accelerating cosmological expansion (see Astier et al. 2006; Riess et al. 2007; Wood-Vasey et al. 2007, for recent applications). Several studies have examined the spread in observed fluxes (rather than their average) due to the magnification of SNeIa as a source of bias in cosmological parameter extraction from the distance–redshift test (Sasaki 1987; Linder et al. 1988; Kantowski et al. 1995; Wambsganss et al. 1997; Holz 1998; Wang 1999; Barber 2000; Holz & Linder 2005), a cross-check of lensing shear maps (Cooray et al. 2006, and references therein), or as an interesting signal in its own right (Metcalf 1999; Dodelson & Vallinotto 2006; Cooray et al. 2006; Albrecht et al. 2006).

The present paper is inspired by these studies and other efforts to explore how SNeIa might be utilized as part of a large, photometric survey (e.g., Albrecht et al. 2006; Zhan et al. 2008; Hannestad et al. 2008; Zhang & Chen 2008). The aforementioned studies considered the lensing of a relatively small ($\lesssim 10^3$) spectroscopic sample of SNeIa, with redshifts that are known precisely (with errors $\lesssim 10^{-4}$, as prescribed by Huterer et al. 2004). We examine the utility of a significantly larger ($\sim 10^6$) photometric sample of supernovae that may be collected by a future, wide, fast, imaging survey such

as the proposed Large Synoptic Survey Telescope (LSST)¹ in which the vast majority of SNeIa will not have accompanying spectroscopic observations. It is thought that the identification and determination of photometric redshifts for SNeIa can be done relatively reliably (Pinto et al. 2004; Wang et al. 2007). Consequently, the dispersion in SNeIa fluxes at fixed *photometric* redshift has three sources: the intrinsic dispersion of SNeIa, including errors in calibrating the standard candles and applying K-corrections and extinction corrections; photometric redshift errors; and any dispersion induced by gravitational lensing. Moreover, each of these factors are thought to contribute to the total dispersion at fixed photometric redshift at comparable levels (see § 2). The implication is that a very large sample of supernovae from an imaging survey can be used to overwhelm the intrinsic dispersion, thus enabling the measurement of SNeIa dispersion induced by photometric redshift errors and gravitational lensing which should shed light on both SNeIa photometric redshifts and cosmological parameters at relatively low redshift.

The modest goal of this paper is to make preliminary estimates of the utility of such a photometric SNeIa sample to learn about cosmology from the dispersion among SNeIa fluxes in conjunction with the traditional distance–redshift test. We find that the spread in observed SNeIa fluxes at fixed redshift provides constraints that are not, by themselves, competitive with other probes (such as weak lensing shear), but are yet interesting, subject to unique systematic errors, and obtained without significant additional observational effort if such a sample is to be used to perform the traditional distance–redshift test or to map baryon acoustic oscillations

¹ <http://www.lsst.org>

(as studied in Albrecht et al. 2006; Zhan et al. 2008). In fact, because such a measurement will be most constraining on dark energy at low redshift ($z \sim 0.2-0.4$) it will have some degree of complementarity with other measures, such as cosmic shear which best constrains the dark energy equation of state near $z \sim 0.7$. More importantly, the information contained in the traditional distance–redshift test (most sensitive to the dark energy equation of state near $z \sim 0.1$) and the dispersion of SNeIa brightnesses complement *each other* and help to make cosmology with photometric SNeIa more robust to uncertainties in photometric redshifts.

Of course, the lack of spectroscopy is a *major* complication in using SNeIa from a photometric survey. As the use of photometric SNeIa samples for cosmology requires some treatment of photometric redshift uncertainties, we also address the dependence of cosmological constraints upon the calibration of SNeIa photometric redshifts. In particular, we find that utilizing the dispersion in SNeIa distance moduli allows for mild self-calibration in the uncertainties of photometric redshift distributions. Perhaps more interestingly, we present results for dark energy constraints as a function of the size of a spectroscopic sample of SNeIa that can be used to calibrate photometric redshifts for two different assumptions about the redshift distribution of this spectroscopic calibration set. This is a convenient way to express cosmological constraints as a function of prior knowledge of the photometric redshift distribution of SNeIa. Interestingly, we find that if the goal is to seek the best constraint on the equation of state parameter at the epoch where it is best constrained by the data (the so-called “pivot” equation of state, see § 2, results are similar for a constant equation of state model), then there is decreasing marginal value in expanding the size of the spectroscopic calibration set beyond a few thousand SNeIa, a number of SNeIa that should be achievable in the coming decade. However, this statement does depend upon model details and upon the assumption that it is the pivot equation of state that is of most interest.

There are several important caveat to our analysis. We neglect the, perhaps considerable, additional complications in supernova type identification and calibration arising from the lack of spectroscopy. Aside from neglect of several potentially-important observational realities, our calculation is also an idealized one. We have treated the influence of gravitational lensing on observed fluxes in a simplified manner, in large part because current analytic models for the proposed lensing signal are not adequate for future surveys and a full treatment of this effect is computationally demanding. However, part of the purpose of this paper is to demonstrate that such a signal does contain valuable information and to emphasize that as we yet lack the theoretical tools needed to perform a robust analysis of future data, developing such tools should be a high priority in the run-up to forthcoming photometric surveys.

The present paper is organized as follows. In § 2 we describe the our treatment of SNeIa observables and photometric redshifts as well as our methods for forecasting cosmological parameter constraints. We present our primary results in § 3. We discuss our results, including implications and important caveats in § 4.

2. BASIS AND METHODS

The average distance moduli μ , of high-redshift supernovae as a function of redshift provide the most direct evidence for cosmological acceleration. In the absence of any lensing, the

distance modulus of a standard candle at true redshift z is $\mu = 5 \log[D_L(z)/10 \text{ pc}]$, where $D_L(z)$ is the luminosity distance to redshift z . We explore both the mean and dispersion in distance moduli of SNeIa measured in a future, large photometric survey. We assume a survey that covers $\approx 20,000 \text{ deg}^2$ to a redshift of $z \sim 0.8$ for 10 years as might be achieved with the LSST instrument and survey strategy. We take a SNeIa redshift distribution dn/dz as in Zhan et al. (2008), which rises to $z \sim 0.5$ ($dn/dz \propto z^{2.1}$ for $z \ll 0.5$) and declines rapidly thereafter ($dn/dz \propto \exp[-32(z-0.5)^2]$ for $z \gg 0.5$). The rate at which supernovae may be discovered and the efficiency with which they will produce light curves suitable for calibration and reliable photometric redshift determination is uncertain and depends upon the exposure strategy of any such survey. For simplicity, we choose a fiducial survey containing one million SNeIa. We note in passing that this normalization is significantly more ambitious than the 3×10^5 SNeIa assumed for the hypothetical, stage IV, ground-based survey explored by the Dark Energy Task Force (DETF, Albrecht et al. 2006), but significantly less ambitious than the 7.4 million SNeIa assumed in the exploration of SNeIa as a tracer of baryon acoustic oscillations by Zhan et al. (2008). In the absence of additional prior constraints on cosmological parameters and external calibration samples of SNeIa (see details below) parameter uncertainties would scale with sample size as $\sigma \propto 1/\sqrt{N_{\text{SNeIa}}}$; however, our constraints scale more slowly because we assume priors on cosmological parameters as well as the availability of additional spectroscopic SNeIa samples that improve the calibration of SNeIa properties and redshifts.

Each observed supernova will be assigned a photometric redshift z_p that is significantly less reliable than could be achieved with spectroscopy. We model photometric redshift uncertainties as follows (Ma et al. 2006). We assume a distribution of photometric redshifts given a spectroscopic redshift $P(z_p|z)$, that is a Gaussian with an offset from the true redshift $b_z(z)$ and dispersion $\sigma_z(z)$, each of which may depend upon redshift. Recent studies indicate that $b_z \approx 0$ and $\sigma_z \approx \sigma_{z0}(1+z)$ with $\sigma_{z0} \approx 0.01$ should be achievable (Pinto et al. 2004; Albrecht et al. 2006; Wang et al. 2007). In practice, it is necessary to allow b_z and σ_z to have significant freedom to vary as a function of z . We do this by representing the functions b_z and σ_z by the values of these functions tabulated at n_{pz} redshifts spaced evenly in z from $z = 0$ to $z = 1.5$ and evaluating these functions at points between the redshifts at which they are tabulated using linear interpolation. Thus there are $2n_{pz}$ photometric redshift parameters. We set n_{pz} by requiring that n_{pz} be large enough that when all $2n_{pz}$ parameters are allowed to vary without prior knowledge, the constraining power of the data converges to a minimum value corresponding to complete lack of redshift information. In practice, our results converge to this minimum with $n_{pz} \approx 15$ and to be conservative, we fix $n_{pz} = 31$ as in the lensing study of Ma et al. (2006) for the remainder of this paper.

Of course, there will be *some* prior knowledge of $P(z_p|z)$ and in principle each of the photometric redshift model parameters will have its own prior. In fact, some calibration of the photometric redshift distribution is needed in order to utilize SNeIa from an imaging survey as we demonstrate explicitly in the following section. For simplicity, we quantify the influence of priors using two one-parameter models that are reasonable, but not exhaustive of all possibilities. We assume a sample of N_{spec} SNeIa with known spectroscopic redshifts. We further assume that this calibration sample either follows

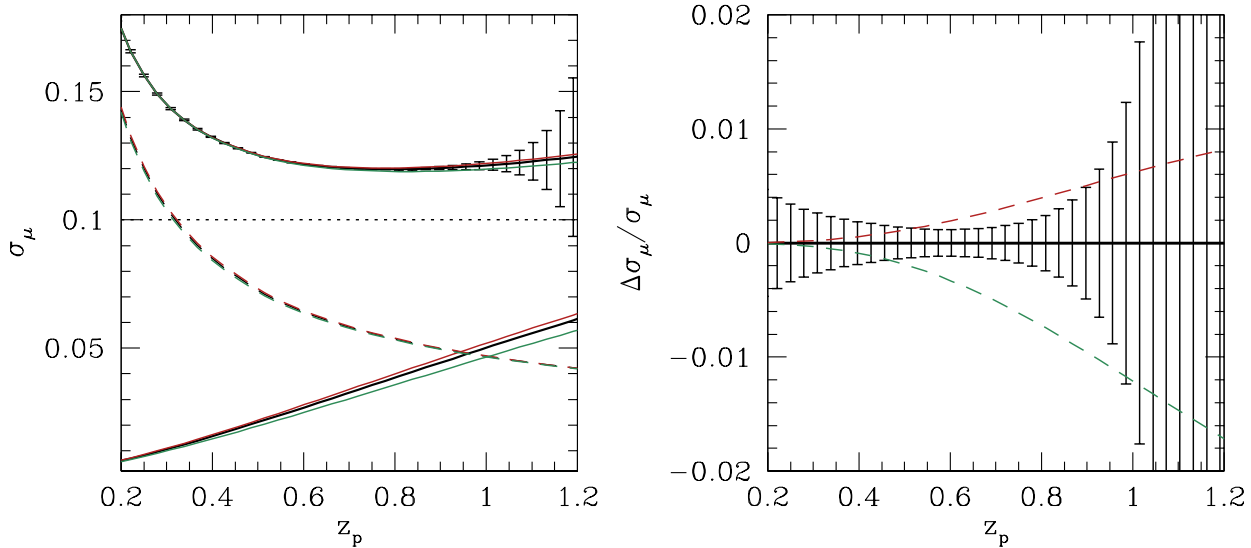


FIG. 1.— The dispersion in supernova distance moduli. *Left*: Dispersion as a function of photometric redshift for SNeIa in 51 bins of photometric redshift. The horizontal, dotted line represents the assumed intrinsic dispersion level of $\sigma_{\text{int}} = 0.1$. A set of three, nearly indistinguishable dashed lines decrease as a function of redshift. These lines represent the contribution to the dispersion from the first two terms in Eq. (4). The central line corresponds to our fiducial cosmological model while the upper (lower) line corresponds to the same cosmology but with $w_0 = -1.1$ ($w_0 = -0.9$). A set of three solid lines increases monotonically with redshift. These represent the contribution to the net dispersion from gravitational lensing. The central line is for our fiducial cosmology, while the upper (lower) line has $w_0 = -1.1$ ($w_0 = -0.9$). The uppermost, solid lines represent the total dispersion in Eq. (4). The central, upper, and lower lines correspond to models with $w_0 = -1$, $w_0 = -1.1$, and $w_0 = -0.9$ respectively, while the errorbars correspond to the statistical error on a determination of each of the 51 $\sigma_{\mu,i}$ from a sample of one million SNeIa. *Right*: Residuals of the dispersion in distance modulus with respect to our fiducial cosmological model with $w_0 = -1$. The upper dashed line is the dispersion in a cosmology with $w_0 = -1.1$ and the lower line is the dispersion with $w_0 = -0.9$. The errorbars are the errors on the measurement of the dispersion in each of 51 photometric redshift bins as in the left panel. This figure is modeled after Figure 1 of Dodelson & Vallinotto (2006) and demonstrates that the dispersion in standard candle distance moduli that may be measured in a forthcoming, large, photometric survey like the LSST will undertake, has some leverage to distinguish dark energy equations of state.

the overall distribution dn/dz , or is spaced uniformly in redshift from $z = 0.1$ to $z = 1.7$ as might be expected from a Joint Dark Energy Mission (JDEM) SNeIa sample² that might be a contemporary of a large-scale photometric survey (Kim et al. 2004; Albrecht et al. 2006). We also incorporate the influence of a nearby sample of SNeIa with spectroscopic redshifts that help to serve as a low-redshift anchor for the distance–redshift test. For this, we take the *nearby* SNeIa sample to contain 500 objects uniformly distributed in the redshift interval $z = 0.03 - 0.08$ with redshift errors of $\sigma_z = 10^{-4}$ as expected from the ongoing Nearby Supernova Factory (Aldering et al. 2002; Copin et al. 2006; Albrecht et al. 2006)³ experiment.

Any calibration set would determine the bias, b_z^i , and dispersion, σ_z^i , of the photometric redshift distribution in redshift bin i with uncertainties of $\sigma_{b_z^i} = \sigma_z^i / \sqrt{N_{\text{spec}}^i}$ and $\sigma_{\sigma_z^i} = \sigma_z^i / \sqrt{2N_{\text{spec}}^i}$ where N_{spec}^i is the number of spectroscopic SNeIa that fall in bin i . We include the influence of prior knowledge of the photometric redshift distribution using such priors. We assume a fiducial model set by $b_z = 0$ and $\sigma_z = \sigma_{z0}(1+z)$ with $\sigma_{z0} = 0.01$. We reiterate that, unless otherwise stated, we allow for uncertainty in the photometric redshift distribution as a function of redshift through the $2n_{\text{pz}}$ photometric redshift parameters and *do not* assume that the photometric redshift parameters are fixed at the fiducial values (in contrast to, for example, Hannestad et al. 2008, who assume perfect knowledge of SNeIa redshifts and Zhan et al. 2008 who do not con-

sider calibration of the bias in photometric redshifts).

For computational convenience, we compute the observable properties of supernovae in bins of photometric redshift. Given the distribution $P(z_p|z)$, the true redshift distribution of SNeIa in photometric redshift bin i is

$$\frac{dn_i}{dz} = \int_{z_p^{\text{low}}}^{z_p^{\text{high}}} \frac{dn}{dz} P(z_p|z) dz_p, \quad (1)$$

where z_p^{low} and z_p^{high} are the lower and upper boundaries of photometric redshift bin i respectively. The total number of SNeIa in photometric redshift bin i is $N_{\text{phot}}^i = \int (dn_i/dz) dz$ and we define the normalized redshift distribution of SNeIa in bin i as $g_i(z) = (dn_i/dz) / N_{\text{phot}}^i$. In practice, we take 51 bins spaced equally in redshift from $z = 0$ to $z = 1.5$. Though convenient considering observables averaged within redshift bins reduces information content relative to the total information available. We have explored various binning schemes and find that finer binning is unnecessary as our results are already converged with this number of bins. In particular, increasing the number of bins by a factor of 3 gives only $\sim 4\%$ better constraints on the pivot dark energy equation of state parameter defined below.

Consider an effective distance modulus defined for convenience to be the difference between apparent magnitude and an assumed average absolute magnitude. Any observed supernova has an effective distance modulus

$$\mu = \Delta + 5 \log \left(\frac{D_L}{10 \text{ pc}} \right) + \delta\mu_{\text{int}} + \delta\mu_{\text{lens}}, \quad (2)$$

where $\delta\mu_{\text{int}}$ is the variation in apparent magnitude due to the intrinsic variations in SNeIa absolute magnitudes, $\delta\mu_{\text{lens}}$ is the

² The Supernova Acceleration Probe (SNAP) is an example, see <http://snap.lbl.gov>

³ <http://snfactory.lbl.gov>

contribution from gravitational lensing, and Δ is some constant offset that is applied to all supernovae and represents a deviation from the assumed average absolute magnitude which includes errors in H_0 . In what follows, we set Δ to vary freely. The average distance modulus of SNeIa in the i^{th} photometric redshift bin is

$$\bar{\mu}_i = \Delta + 5 \int dz g_i(z) \log \left[\frac{D_L(z)}{10 \text{ pc}} \right] \quad (3)$$

and the standard distance–redshift test is an application of this relation. In addition to distance modulus, the Greek letter “ μ ” is also the conventional symbol for the lensing magnification. In order to avoid confusion, we will *not* refer to the lensing magnification directly but only to the shift in distance modulus induced by weak gravitational lensing.

The dispersion in the effective distance modulus $\sigma_{\mu,i}$, is given by

$$\sigma_{\mu,i}^2 = 25 \left(\int dz g_i(z) \log^2 \left(\frac{D_L}{10 \text{ pc}} \right) - \left[\int dz g_i(z) \log \left(\frac{D_L}{10 \text{ pc}} \right) \right]^2 \right) + \int dz g_i(z) \sigma_{\text{int}}^2(z) + \int dz g_i(z) \sigma_{\text{lens}}^2(z), \quad (4)$$

where σ_{int} is the intrinsic dispersion of SNeIa brightnesses, which may itself vary with redshift, and σ_{lens} is the dispersion induced by gravitational lensing. The first two terms in parenthesis in Eq. (4) represent the spread in observed SNeIa distance moduli due to the spread in photometric redshifts.

In the weak lensing limit (convergence $\kappa \ll 1$), the dispersion due to lensing is (Bernardeau et al. 1997; Valageas 2000; Dodelson & Vallinotto 2006)

$$\sigma_{\text{lens}}^2(z) = \frac{225 \Omega_M^2 H_0^2}{8\pi \ln^2(10)} \int_0^z dz' \frac{W^2(z', z)}{H(z)} \times \int dk k P(k, z') \mathcal{W}_{\text{TH}}^2(D_A k \theta_s), \quad (5)$$

where $W(z', z) = H_0 D_A(z') D_A(z', z) / D_A(z)$, $D_A(z)$ is the angular diameter distance to redshift z , and $D_A(z', z)$ is the angular diameter distance between redshifts z' and z . The quantity $P(k, z)$ is the matter power spectrum and we evaluate it using the relation of Smith et al. (2003). The function $\mathcal{W}_{\text{TH}}(x) = 2J_1(x)/x$ in Eq. (5) is a smoothing function that arises by considering the magnification averaged over an angular tophat of radius $\theta_s \ll 1$. In practice, we set $\theta_s = 1''$, but the choice is relatively unimportant in that $D_A k \theta_s \ll 1$ and so $\mathcal{W}_{\text{TH}}(D_A k \theta_s) \simeq 1$ for relevant choices of θ_s . We assume the lensing to be uncorrelated (Metcalf 1999; Cooray et al. 2006; Dodelson & Vallinotto 2006) and take the $\sigma_{\mu,i}$ as an independent set of observables that can be extracted from the observed SNeIa population.

Figure 1 shows the dispersion in distance modulus in 51 photometric redshift bins as a function of the center of the photometric redshift bin z_p in our fiducial cosmological model. Our fiducial model has $\omega_M = 0.13$, $\omega_B = 0.0223$, $\Omega_k = 0$, $\Delta_{\mathcal{R}}^2 = 2.47 \times 10^{-9}$, and $n_s = 1$. We describe dark energy by its present energy density $\Omega_{\text{DE}} = 0.76$ and a time-varying equation of state parameter $w(a) = w_0 + w_a(1-a)$, with $w_0 = -1$ and $w_a = 0$ in our fiducial model. For the purpose of this illustration, we take $\sigma_{\text{int}} = 0.1$. We will return to the intrinsic dispersion later. Notice that the contributions to the dispersion due to the photometric redshift distribution and gravitational lensing are comparable and give the total dispersion a characteristic dependence upon redshift. In particular, the dispersion

decreases at low redshift and increases at high redshift due to the increased dispersion due to lensing. This makes it possible to use the dispersion to extract cosmological information without a good constraint on the level of the intrinsic dispersion.

We estimate constraining power using a Fisher matrix analysis. The Fisher matrix formalism is ubiquitous in cosmological parameter forecasting (useful references include Jungman et al. 1996; Tegmark et al. 1997; Seljak 1997; Metcalf 1999; Albrecht et al. 2006; Zhan et al. 2008, the last three of which explore cases similar to the present paper) and so we will not review the formalism here. We take as our ob-servables the set $\bar{\mu}_i$ and $\sigma_{\mu,i}$ with errors of $\sigma(\bar{\mu}_i) = \sigma_{\mu,i} / \sqrt{N_{\text{phot}}^i}$

and $\sigma(\sigma_{\mu,i}) = \sigma_{\mu,i} / \sqrt{2N_{\text{phot}}^i}$ respectively. We refer to constraints using the $\bar{\mu}_i$ alone as “luminosity distance test,” and constraints from the $\sigma_{\mu,i}$ alone as the “dispersion test.” The Fisher matrix F_{mm} , approximates the covariance in model parameters locally about the maximum likelihood, so the indices run over the parameters in the parameter space we seek to constrain. The 1σ constraint on parameter p is approximated by the square root of the diagonal component of the inverse Fisher matrix corresponding to this parameter. We denote this $\sigma(p) \simeq \sqrt{[F^{-1}]_{pp}}$. Along with the parameters Δ and σ_{int} describing SNeIa and the parameters describing the photometric redshift distribution, we vary the eight cosmological parameters in the previous paragraph about their quoted fiducial values. We take independent, Gaussian priors on these parameters of $\sigma(\omega_M) = 0.004$, $\sigma(\omega_B) = 6 \times 10^{-4}$, $\sigma(\Omega_k) = 10^{-3}$, $\sigma(\ln \Delta_{\mathcal{R}}^2) = 0.04$, and $\sigma(n_s) = 0.02$, all of which are comparable to contemporary constraints on these parameters (Komatsu et al. 2008).

Absent significant direction from theory, it is not clear how to assess the constraining power of a dark energy program. We use two reasonable metrics. First, we consider the area of the marginalized 95% error ellipse in the w_0 – w_a plane \mathcal{A} , as suggested by the DETF (Albrecht et al. 2006, the DETF actually uses $1/\mathcal{A}$, see also Huterer & Turner 2001 for a similar suggestion). Alternatively, it may be supposed that the goal of a dark energy experiment should be primarily to limit any deviation from a vacuum energy or cosmological constant, both of which have constant $w = -1$. In this case, it is interesting to examine the error on the equation of state parameter $w(a)$ at the epoch where it is most well constrained, the so-called pivot scale factor a_p or pivot redshift $z_{\text{piv}} = 1/a_p - 1$ (e.g., Huterer & Turner 2001; Hu & Jain 2004; Albrecht et al. 2006). The pivot scale factor is $a_p = 1 + [F^{-1}]_{w_0 w_a} / [F^{-1}]_{w_a w_a}$. The corresponding pivot equation of state is $w_p = w_0 + (1 - a_p)w_a$, so the error on w_p is $\sigma^2(w_p) = [F^{-1}]_{w_0 w_0} - [F^{-1}]_{w_0 w_a}^2 / [F^{-1}]_{w_a w_a}$. The parameters w_p and w_a are uncorrelated and the transformation from a w_0 – w_a parameterization preserves the area of the error ellipse in the two parameters, so $\mathcal{A} \simeq 6.17\pi\sigma(w_p)\sigma(w_a)$.

Our estimate of parameter uncertainties stands as one of many abuses of the Fisher matrix that appear in the literature and this warrants some discussion. For one thing, we expect the likelihood to be non-Gaussian for an interesting range of parameter values (though Metcalf 1999, also works in the Gaussian approximation, see also § 4). More importantly, we consider only the mean [Eq. (3)] and dispersion [Eq. (4)], rather than the full μ distribution. In principle, one would like to, and should, account for the full shape of the distribution of μ , which is non-Gaussian in large part because

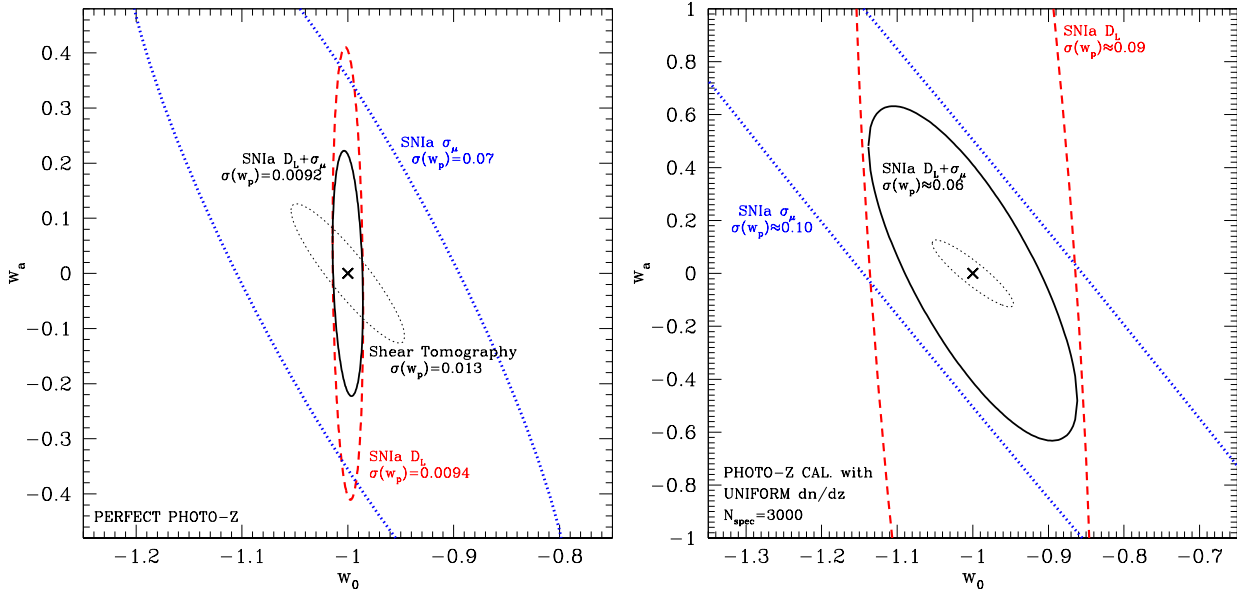


FIG. 2.— Constraint contours in the w_0 - w_a plane. The *left* panel shows 1σ constraint contours in the limit of perfect knowledge of the parameters of the photometric redshift model. The *right* panel shows parameter constraints assuming priors on the photometric redshift parameters that would be obtained after calibrating to a spectroscopic sample of $N_{\text{spec}} = 3000$ SNeIa distributed uniformly in redshift over the interval $0.1 \leq z \leq 1.7$. Note that the axes in the two panels span different ranges. In each panel, the cross marks the fiducial model with $w_0 = -1$ and $w_a = 0$. The *outer, dashed* contours represent the dark energy constraints from the standard luminosity distance–redshift test [Eq. (3)] alone. The *outer, dotted* contours represent constraints from the dispersion among SNeIa alone. The *solid* contours show the combined constraints from both the mean and dispersion among SNeIa distance moduli. To set these constraints in context, the *inner, thin, dotted* contours in each panel show the constraints expected from galaxy weak lensing shear tomography in an LSST-like survey computed using the same fiducial model as described in Zentner et al. (2008).

the distribution of magnifications due to lensing is strongly non-Gaussian (e.g., Schneider & Wagoner 1987; Sasaki 1987; Wambsganss et al. 1997; Holz 1998; Wang 1999; Valageas 2000; Munshi & Jain 2000; Wang et al. 2002). One way to see that lensing should be non-Gaussian is to recognize that a minimum amount of de-magnification (or dimming) will occur when the null geodesic passes through an empty beam with density $\rho = 0$. The minimum magnification of a source at redshift z_s , corresponds to a maximum shift in distance modulus of $\delta\mu_{\text{max}} = (15/2)\Omega_M H_0 \int_0^{z_s} dz W(z, z_s)/H(z)$. There is no corresponding upper limit to magnification or corresponding lower limit to $\delta\mu_{\text{lens}}$.

We use the Fisher matrix formalism and consider only the dispersion in μ as a matter of pragmatism. First, computing the distribution of magnifications due to lensing is computationally intensive and still subject to uncertainties in numerical modeling of nonlinear structure formation (e.g., Huterer & Takada 2005; Hagan et al. 2005; Rudd et al. 2008) at levels that are important for forthcoming data. Neglecting systematic issues, this problem could be circumvented if a reliable, analytic fitting form for the magnification distribution could be used. Wang et al. (2002) provide such a fit, but we find that the Wang et al. (2002) relation is neither sufficiently accurate to address forthcoming large data sets (\sim percent-level predictions are necessary), nor is it internally self-consistent below redshifts $z \sim 0.6$, where the probability density of magnification exhibits discontinuities and violates flux conservation⁴. This is particularly important for the

⁴ The redshifts at which these issues of inconsistency become important vary considerably with cosmological parameters. These issues are alluded to in the work of Dodelson & Vallinotto (2006), but they do not specify the shortcomings of the Wang et al. (2002) fitting form. The shortcomings are understandable in the sense that the present application was likely not fore-

present study because the bulk of SNeIa in any ground-based, photometric survey of a large fraction of the sky will be at redshifts $\lesssim 0.6$.

If such a fitting form were available, the present study with $\sim 10^6$ SNeIa and ~ 70 parameters would still be computationally demanding. What one would like to do is to perform a Monte-Carlo analysis (as was done in Dodelson & Vallinotto 2006) in which random realizations of SNeIa fluxes are generated and to map out the likelihood during a random walk through the parameter space (e.g., Christensen & Meyer 2001; Christensen et al. 2001; Knox et al. 2001; Kosowsky et al. 2002). In doing so, one would also treat the full lensing distribution, rather than taking the weak lensing limit (where convergence $\kappa \ll 1$ or $\delta\mu_{\text{lens}} \ll 1$), which does not account properly for the objects in the high-magnification tail of the lensing distribution. Dodelson & Vallinotto (2006) and Sarkar et al. (2008b) have shown that working in this limit does induce biases in cosmological parameters inferred from any observational data sets, but does not significantly alter parameter constraints. Indeed, we note here that we have successfully repeated the Monte Carlo analysis of Dodelson & Vallinotto (2006), finding similar results. We have also performed the same Monte Carlo analysis for our photometric survey in cases of a reduced parameter space where the photometric redshift distribution is assumed to be known perfectly and in which only Ω_M and w_0 vary. In both cases, a Fisher matrix analysis yields constraints that are in rough agreement ($\sim 30\%$) with the more complete approach. Detailed and precise theoretical predictions and detailed survey strategies and systematics analyses

seen by Wang et al. (2002), so it seems reasonable that these authors would not expend significant effort to calibrate their fit at low redshifts.

are not yet available, so we do not consider a calculation that incorporates a full Monte Carlo analysis of the lensing distribution and the parameter space to be warranted at present and, for practical reasons, we have not performed such a calculation. However, any analysis of an observational data set must undertake such a calculation.

Rather than treating such a specific calculation, our point is to indicate that the dispersion among supernovae in any large photometric survey that also aims at using the SNeIa sample to perform the distance–redshift test, measure baryon acoustic oscillations, or even assess SNeIa systematics will be a source of meaningful information. In fact, part of our point is that such information may be present in future data, but the theoretical tools to do a rigorous analysis of such data are lacking and must be developed. We return to many of these issues in § 4.

3. RESULTS

This section contains our results regarding the utility of a large, photometric sample of SNeIa to constrain cosmological parameters. Our primary interest is in the ability of SNeIa to constrain the dark energy equation of state, and so we focus our attention on w_0 , w_a , the pivot value of the equation of state parameter w_p , and the 95% w_0 – w_a ellipse area \mathcal{A} . We illustrate the general utility of SNeIa from a large photometric survey, and in particular the utility of examining both the mean and dispersion among distance moduli, in Figure 2.

The left panel of Fig. 2 shows constraints in the unrealistically-optimistic situation where the parameters of the photometric redshift model are known perfectly. In reality, this cannot be the case, but this represents the limit of the best possible cosmological constraints that could be achieved with a photometric survey of supernovae. We present results for a fiducial case with 10^6 supernovae. We reiterate that for a fixed redshift distribution and in the absence of external priors, constraints would scale with the total number of supernovae as $\sigma \propto 1/\sqrt{N_{\text{SNe}}}$ and this could be used to scale constraints to approximate those from smaller or larger samples with similar redshift distributions (e.g., Albrecht et al. 2006; Hannestad et al. 2008; Zhan et al. 2008). Our constraints scale somewhat more slowly due to the influence of the external priors we assume.

There are several things to note in the left panel of Fig. 2. First, in the limit of perfect knowledge of the photometric redshift distribution and perfect control of systematic uncertainties, constraints from the standard luminosity distance test dominate, placing a constraint on w_p of $\sigma(w_p) \simeq 0.01$. However, the extra information contained in the SNeIa dispersions is not uninteresting. The dispersion test constrains the pivot equation of state parameter to $\sigma(w_p) \simeq 0.07$ by itself. More importantly though, is that the luminosity distance and dispersion contain complementary information. The luminosity distance test alone has a pivot redshift of $z \sim 0.1$, and so the constraint contours from this test alone are quite vertical. The dispersion test has a pivot redshift at $z \sim 0.4$, and so the dispersion contours are more inclined and it is clear that the dispersion test complements the distance test. The combined constraint from the mean and dispersions among supernovae distance moduli result in a constraint on w_p that is only slightly smaller than that from the distance test alone, but a significant reduction in the area of the 95% contour by a factor of roughly ~ 2 . For reference, we also show constraints from weak lensing shear tomography for the LSST survey as estimated by Zentner et al. (2008), assuming photometric redshift calibra-

tion with a spectroscopic sample of 10^5 galaxies as in Model I of Ma et al. (2006). The weak lensing constraint on w_p is $\sigma(w_p) = 0.013$, weaker than that from SNeIa in this idealistic scenario, but the area of the 95% contour for weak lensing shear tomography is about 30% smaller than that from SNeIa. Aside from serving as a reference, this also demonstrates in a tangible way that the criteria of minimizing $\sigma(w_p)$ and \mathcal{A} can result in notably different conclusions. In what remains, we make an effort to address constraints in a variety of more plausible scenarios.

The right panel of Fig. 2 depicts 1σ constraint contours in the more realistic case of imperfect knowledge of the photometric redshift parameters. As described in § 2, we quantify the knowledge of the photometric redshift parameters in terms of the size of the spectroscopic sample used to place priors on these parameters, N_{spec} . For the specific results in the right panel of Fig. 2, we have chosen $N_{\text{spec}} = 3000$ and assumed the spectroscopic calibration sample to be distributed uniformly in redshift over the range $0.1 \leq z \leq 1.7$, as might result from a forthcoming JDEM (Kim et al. 2004; Albrecht et al. 2006). Note that the axes on the right panel of Fig. 2 span a different range from the left panel, but that the inner contour showing projected constraints from galaxy shear tomography are identical in each panel.

The right panel of Fig. 2 shows a considerable degradation of dark energy constraints from either the standard test of luminosity distance or the dispersion of SNeIa distance moduli alone relative to the case of perfect knowledge of the photometric redshift distribution. This demonstrates the importance of both a realistic assessment of photometric redshift uncertainties and prior information to constrain photometric redshifts. However, this panel also depicts the complementary nature of these constraints. The luminosity distance test alone gives an error on the pivot equation of state parameter of $\sigma(w_p) \approx 0.09$. Utilizing the information contained within the dispersion of SNeIa as well as the mean decreases the error on the pivot equation of state parameter to roughly $\sigma(w_p) \simeq 0.06$ and decreases the area of the 95% contours relative to either test individually by nearly a factor of ten by breaking the prominent degeneracy in the w_0 – w_a parameter space. Worthy of note is the fact that at this level, the constraints from the large, photometric SNeIa sample are comparable to the constraints expected from the spectroscopic sample used for photometric redshift calibration (see also Albrecht et al. 2006), so they are both interesting and relevant, but the availability of a significantly larger spectroscopic sample would obviously be more valuable because of the constraints it can place on dark energy directly, rather than its ability to calibrate the redshifts of a photometric sample.

Though Fig. 2 shows contours in two simple models, the basic point is that SNeIa dispersions derived from forthcoming large, photometric surveys are potentially useful. Generally, the luminosity distance test is subject to a strong degeneracy between w_0 , w_a , and Ω_M . Our choice of priors mitigates the influence of Ω_M , but the w_0 – w_a degeneracy remains because the sample has only a relatively small redshift span and therefore limited leverage with which to measure any time variation of the dark energy equation of state. Some contemporary studies and several future proposals for SNeIa-based dark energy experiments (such as a Joint Dark Energy Mission like SNAP) aim to break this degeneracy by observing high-redshift survey (e.g., Riess et al. 2007). On the contrary, our assumed photometric survey has no high-redshift component. In fact, the number of SNeIa in our assumed survey de-

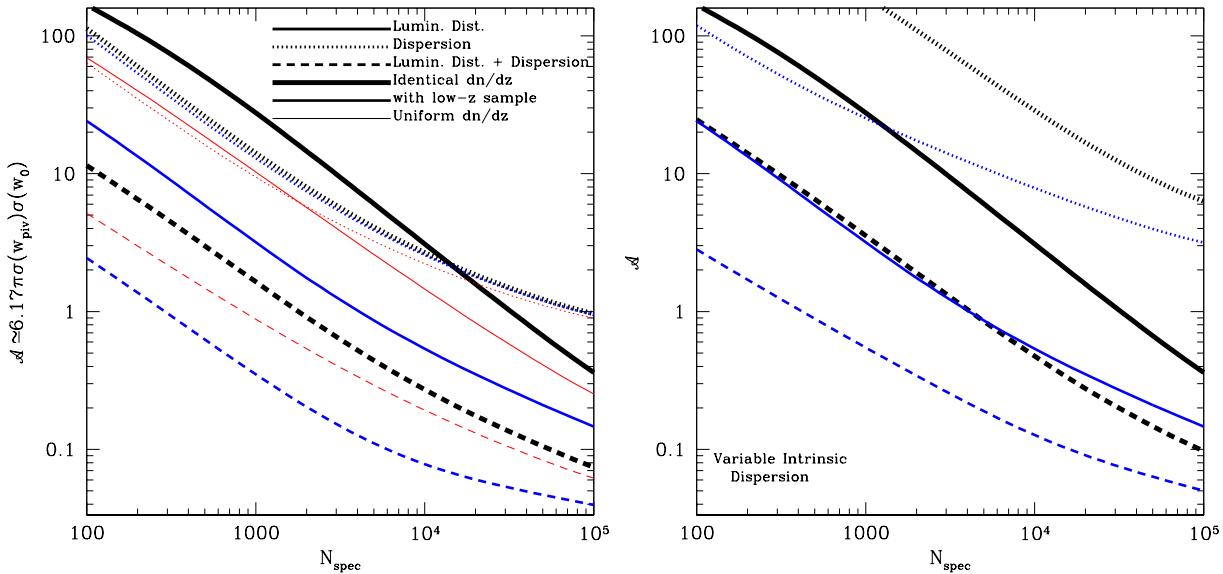


FIG. 3.— Influence of spectroscopic calibration sets on dark energy constraints from a large sample of SNeIa from a photometric survey. This plot depicts the area of the 95% contour in the w_0 - w_a plane \mathcal{A} , as a function of the size of the spectroscopic SNeIa sample used to calibrate the photometric redshift model, under several assumptions. There are nine lines in the *left* panel. The *solid* lines represent constraints as a function of spectroscopic sample size from the luminosity distance–redshift test only. The *dotted* lines represent constraints from the dispersion among SNeIa distance moduli. For each line type, the *thickest* lines show results in a standard case where the spectroscopic calibration sample traces the redshift distribution of SNeIa in the photometric survey. Alternatively, the *thinnest* lines show \mathcal{A} under the assumption that the calibration sample is distributed uniformly in redshift over the interval $z = 0.1 - 1.7$. The lines of *intermediate* thickness show constraints with a spectroscopic sample of size N_{spec} in addition to a low-redshift “nearby” spectroscopic sample of 500 SNeIa distributed uniformly in the interval $z = 0.03 - 0.08$. The *left* panel shows the case of a known and fixed intrinsic dispersion and the *right* panel shows the case of a variable intrinsic dispersion. Note that in the case of a known intrinsic dispersion, the low-redshift, nearby SNe add little information to the dispersion only test, so the dispersion-only lines in these cases are nearly coincident. For clarity, in the *right* panel, we show only two cases, that of the standard sample and that of the standard sample with an additional, nearby spectroscopic sample.

clines rapidly for $z \gtrsim 0.6$ and only a few percent of the SNeIa in the survey have $z \gtrsim 0.8$ (see Zhan et al. 2008). Within the photometric survey, the w_0 - w_a degeneracy is broken by the complementarity between the dispersion due to gravitational lensing and the standard luminosity distance test. This is a potential aspect of complementarity between spectroscopic SNeIa samples and samples from a large, ground-based, photometric survey. The latter, bereft of high-redshift ($z \gtrsim 0.8$) objects, will be sensitive to $w(a)$ at lower redshifts than proposed spectroscopic SNeIa projects that typically extend to $z \gtrsim 1.5$. Moreover, the dispersion test probes the inhomogeneities in the universe. As such, the dispersion test probes a fundamentally different manifestation of dark energy, namely its influence on cosmic structure growth, that is not probed by the luminosity distance test.

A further benefit of the additional dispersion information is that it helps to break degeneracies between cosmological and photometric redshift parameters. In fact, when only considering the canonical luminosity distance test, the only constraints on the photometric redshift parameters come from the priors determined by the photometric redshift calibration set. When both pieces of information are exploited, the data provide for weak “self-calibration,” determining many of the photometric redshift parameters with uncertainties a factor of $\sim 2 - 5$ more stringently than the priors alone. Moreover, Fig. 2 also shows that the dispersion test is less sensitive to photometric redshift uncertainties and degrades more slowly with decreasing knowledge of the photometric redshift distribution. This useful and interesting result stems primarily from the fact that the lensing kernel $[W(z', z)]$ in Eq. (5) is inherently broad and

the dispersion is a comparably mild function of redshift.

As *some* spectroscopic calibration of photometric redshifts is necessary in order to utilize a photometric SNeIa sample, it is interesting to consider potential constraints both as a function of the uncertainty in photometric redshift parameters and under a variety of assumptions about what additional SNeIa data will be available. This permits an estimate of the utility of SNeIa from a future large-scale, photometric survey given specific photometric redshift calibration programs and additional calibration data sets. For this reason, the final two plots of this section present results for dark energy parameter constraints as a function of spectroscopic SNeIa calibration sample size N_{spec} , under a variety of assumptions about additional available data.

First, we consider the area of the 95% ellipse in the w_0 - w_a plane \mathcal{A} , as a function of spectroscopic calibration sample size, N_{spec} . This quantity is shown in Figure 3 for several different combinations of data and model assumptions. In the left panel of Fig. 3, we display results for models in which the intrinsic dispersion is set to a fixed value and in the right panel, for models in which the intrinsic dispersion level is free to float. The thickest lines in Fig. 3 show our standard model constraints with no nearby SNeIa sample and a calibration set distributed in redshift in a manner identical to the SNeIa in the photometric sample. The intermediate thickness lines show \mathcal{A} as a function of N_{spec} in a model that includes the nearby sample of SNeIa. The thinnest lines in Fig. 3 represent the standard model with a calibration set that is distributed uniformly in redshift in the interval $0.1 \leq z \leq 1.7$. For illustrative purposes, we show constraints for spectroscopic sample sizes up

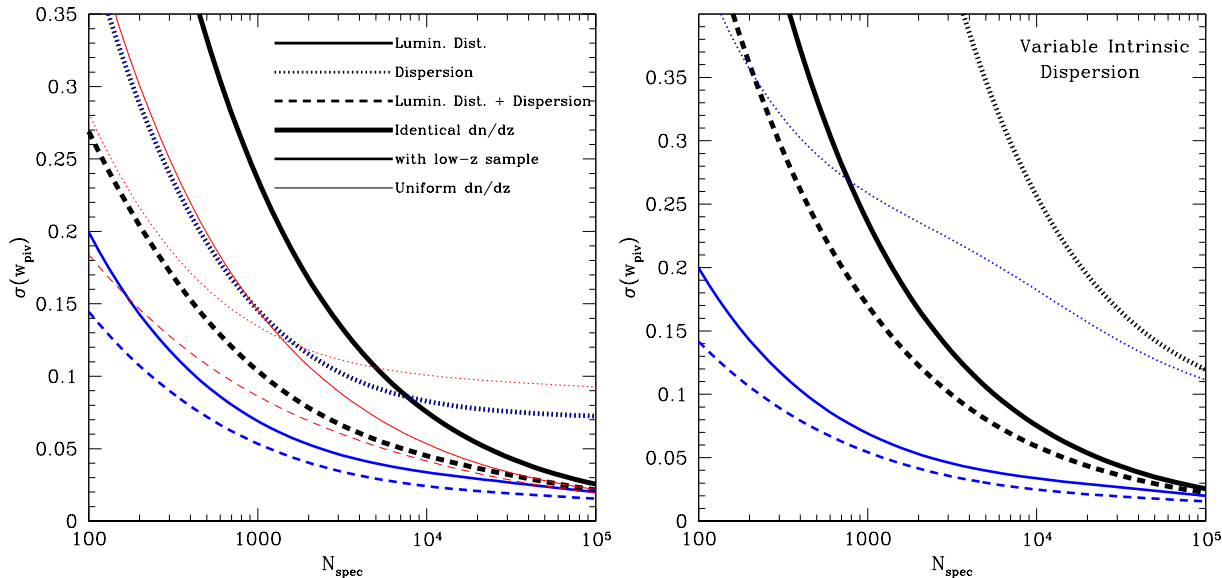


FIG. 4.— Constraints on the dark energy pivot equation of state from a large sample of SNeIa from a photometric survey as a function of the size of the spectroscopically-observed SNeIa set available to calibrate photometric redshifts. This plot depicts constraint on w_p as a function of the size of the spectroscopic sample used N_{spec} , under several assumptions. There are nine lines in the *left* panel. The *solid* lines represent constraints as a function of spectroscopic sample size from the luminosity distance–redshift test only. The *dotted* lines represent constraints from the dispersion among SNeIa distance moduli. The *dashed* lines show the total constraint from both the mean and dispersion in SNeIa distance moduli. For each line type, the *thickest* lines show the results from a standard case where the redshift distribution of the spectroscopic calibration sample traces the redshift distribution of SNeIa in the imaging survey. The *thinnest* lines show $\sigma(w_p)$ assuming that the calibration sample is distributed uniformly in redshift across the interval $z = 0.1 - 1.7$. The lines of *intermediate* thickness show constraints with a spectroscopic sample of size N_{spec} in addition to a low-redshift “nearby” spectroscopic sample of 500 SNeIa distributed uniformly over the interval $z = 0.03 - 0.08$. The *left* panel shows the case of a known and fixed intrinsic dispersion and the *right* panel shows the case of a variable intrinsic dispersion. Note that in the case of a known intrinsic dispersion, the low-redshift, nearby SNe add little information to the dispersion only test, so the dispersion-only lines in these cases are nearly coincident. For clarity, in the *right* panel, we show only two cases, that of the standard sample and that of the standard sample with an additional, nearby spectroscopic sample.

to $N_{\text{spec}} = 10^5$; however, we note that such high N_{spec} are of limited practical interest because an upper limit on achievable spectroscopic sample sizes is $N_{\text{spec}} \sim 10^4$ and at such large N_{spec} constraints from the spectroscopic sample itself begin to dominate any added information from the photometric sample. Note that in Fig. 3 the lines that delineate constraints from the dispersion test only in the standard case and in the case with an additional nearby SNeIa sample are nearly coincident, and may not be readily discernible. The reason for this is simple. Under the assumption that the dispersion is known, the nearby sample does not serve to calibrate the intrinsic dispersion and adds little information.

The complementarity of the information contained in the mean, $\bar{\mu}_i$, and the dispersion, $\sigma_{\mu,i}$, is apparent in Fig. 3. The information contained in SNeIa dispersions is not negligible and in some cases the constraints from SNeIa dispersions can exceed those from the luminosity distance test alone in the regime $N_{\text{spec}} \lesssim 10^4$. The most interesting cases are likely those where the intrinsic dispersion is not known at the outset and/or where there is a nearby SNeIa sample available. In these cases, the information from the standard luminosity distance test alone yields a significantly lower area \mathcal{A} , than the information from the dispersion among distance moduli. Combining constraints from both the mean and the dispersion information drives \mathcal{A} down by roughly a factor of ten compared to either alone in all cases. This is a manifestation of the fact that these two observables are most effective probes at different redshifts and so exhibit different degeneracies in the w_0 - w_a plane (see Fig. 2). In addition, Fig. 3 illustrates that constraints from $\sigma_{\mu,i}$ degrade more slowly with decreasing

N_{spec} than do constraints from the standard luminosity distance test, a feature already evident in Fig. 2.

In general, including the low-redshift, nearby SNe sample drives constraints considerably lower (Aldering et al. 2002; Copin et al. 2006; Albrecht et al. 2006), greatly increasing the utility of the luminosity distance test while only yielding a slight improvement on the dispersion test *if* the intrinsic dispersion level is assumed to be known. Assuming a calibration set of spectroscopically-observed SNeIa that is distributed uniformly in redshift is moderately more powerful than the calibration set that follows the redshift distribution of the SNeIa in the photometric sample. This is because the uniform redshift distribution allows for more accurate photometric redshift calibration at high z_p . This is important for two reasons. First, deviations between observables predicted by different models are larger at high redshift. Second, the redshift distribution of SNeIa dn/dz is a steep function of redshift, dropping as $dn/dz \propto \exp[-32(z-0.5)^2]$ at $z \gg 0.5$, so the scatter of SNeIa in this regime to higher redshift due to redshift errors can lead to significant contamination and a Malmquist-type bias. In all cases, \mathcal{A} continues to decline rapidly with N_{spec} . In principle, this rate of decline levels off as knowledge of photometric redshift distributions become so accurate as to allow for the recovery of all available cosmological information. This drives all of the constraints to begin to converge at large N_{spec} . In practice, this saturation is not achieved until $N_{\text{spec}} \sim 3 \times 10^6$, a limit that is so large as to be uninteresting (it is larger than the photometric SNeIa sample!).

The right panel differs from the left in that the intrinsic

sic dispersion level σ_{int} , is treated as unknown and permitted to vary along with Δ , the cosmological parameters, and the photometric redshift parameters. This leads to considerable degradation in the utility of the dispersion alone to constrain dark energy, but in this case the dispersion information constrains the intrinsic dispersion, determining it to $\sigma(\sigma_{\text{int}}) \simeq 1.6 \times 10^{-3}$. For comparison, we have evaluated the ability of either the nearby sample or a spectroscopic sample with 3000 SNeIa spread uniformly over the redshift interval $0.1 \leq z \leq 1.7$ and redshift errors of $\sigma_z = 10^{-4}$ to constrain σ_{int} . We find that determinations from such data are similar to, but slightly less restrictive, than that from the photometric survey after marginalizing over all other parameters. Conversely, much of the loss of information due to a varying level of intrinsic dispersion is largely *recovered* in the case where the nearby SNeIa sample is included. Notice that complementarity between the information in $\bar{\mu}_i$ and $\sigma_{\mu,i}$ leads to considerable improvements in \mathcal{A} in all cases.

Another useful measure of the constraining power of any set of observables is the error on the equation of state parameter at the pivot redshift, $\sigma(w_p)$. We show the dependence of $\sigma(w_p)$ upon N_{spec} in Figure 4. First, note that $\sigma(w_p)$ varies over a smaller dynamic range than \mathcal{A} , so Fig. 4 has an ordinal axis with a linear scale as opposed to the logarithmic scale used in Fig. 3. After accounting for this difference there are yet some qualitative differences in the behavior of $\sigma(w_p)$ relative to \mathcal{A} . In the limit of small N_{spec} and in the absence of a large, low-redshift, nearby sample of SNeIa the dispersion information can give useful, independent constraints on w_p . Moreover, the dispersion information is generally less useful for improving $\sigma(w_p)$ than it is for improving the \mathcal{A} figure of merit, particularly when the photometric redshift parameters are very well known or the nearby SNeIa sample is available. In these cases, \mathcal{A} improves because the error ellipses are oriented at a significant angle relative to each other, but the shortest axis (the constraint on w_p) is largely determined by the luminosity distance test alone. Lastly, it is worthwhile noting that in the case where there is an available nearby spectroscopic sample, the marginal improvement in w_p upon adding additional objects to the spectroscopic photometric calibration sample is relatively small beyond $N_{\text{spec}} \sim 2 \times 10^3$.

To this point, we have considered cases in which the intrinsic dispersion of SNeIa does not vary with redshift. It is not unlikely that the intrinsic dispersions in SNeIa will change with redshift. For example, SNeIa will be observed in different bands relative to their rest frames at different redshifts with the consequence that standard candle calibration will be a function of redshift (e.g., Hamuy et al. 1995; Prieto et al. 2006). In addition, there is evidence that the Ia class of supernovae is composed of distinct sub-classes and the relative mix of these sub-classes is expected to change with redshift (Hamuy et al. 1995; Howell 2001; Howell et al. 2007). Clearly, if the intrinsic dispersion is allowed to be an *arbitrary* function of redshift, the utility of the added dispersion information is completely eliminated as a cosmological probe. However, we have considered a less pathological case of a redshift-dependent intrinsic dispersion that is monotonic and follows a power-law.

To be specific, we considered a model with $\sigma_{\text{int}}(z) = \sigma_{\text{int},0}(1+z)^\beta$ with both $\sigma_{\text{int},0}$ and β parameters that are fixed by the data ($\beta = 0$ in the fiducial model about which we perturb). We do not show the results in Fig. 3 or Fig. 4 for clarity, but note that further degradation is not devastating. In particular, in the case with no nearby sample, further degradation by

allowing for $\sigma_{\text{int}}(z)$ to vary as a power law in $(1+z)$ is a factor of ~ 2.5 in \mathcal{A} and $\sim 18\%$ in $\sigma(w_p)$ relative to the case of constant σ_{int} . With a nearby spectroscopic sample, $\sigma_{\text{int}}(z)$ at low redshift can be effectively determined and the degradation relative to the case of a redshift-independent intrinsic dispersion is only $\sim 60\%$ in \mathcal{A} and just $\sim 10\%$ in $\sigma(w_p)$. In addition, these data would limit β with uncertainties of $\sigma(\beta) \simeq 0.22$ and $\sigma(\beta) \simeq 0.09$ in cases with and without the nearby sample respectively, a level that is again comparable to the forecasts from a spectroscopic sample. Moreover, it is clear that the lensing contribution to the dispersion must be accounted for in order to extract the intrinsic SNeIa properties. In summary, though the information loss in cases of redshift-dependent intrinsic dispersion is not insignificant, SNeIa in a large, photometric survey can bring significant constraining power to bear on dark energy even with moderate, and poorly-understood time variation of the intrinsic dispersion. Of course, to the degree that the distribution of distance moduli varies markedly and rapidly with redshift outside of the expected range, this distribution will provide a useful handle on the SNeIa properties themselves, including perhaps the evolution of SNeIa and SNeIa population demographics (e.g., Hamuy et al. 1995; Howell 2001; Mannucci et al. 2006; Sullivan et al. 2006; Howell et al. 2007; Sarkar et al. 2008a).

4. IMPLICATIONS AND CAVEATS

We have studied simultaneous constraints on dark energy coming from both the evolution of the mean luminosity distance of SNeIa as a function of redshift and the dispersion among SNeIa fluxes in a SNeIa data set that may arise from a large, wide, and fast photometric survey such as that proposed for the LSST. Sources of dispersion among the measured fluxes of SNeIa in such a survey include intrinsic dispersion among SNeIa (including standard candle calibration), uncertainty in photometric redshifts, and magnification due to gravitational lensing. We have shown that the additional dispersion information complements the traditional luminosity distance test in several ways.

First, the dispersion information breaks a degeneracy between the contemporary dark energy equation of state w_0 , and dark energy equation of state evolution, parameterized here by the common, benchmark parameter w_a . Using the luminosity distance (mean flux) test alone, this degeneracy can be broken by observing high-redshift SNeIa to increase the lever arm of the data in redshift. The dispersion information leads to constraints that break the degeneracy between w_0 and w_a without the need for a high-redshift ($z \gtrsim 0.8$) SNeIa sample (see Fig. 2).

Second, photometric surveys require some calibration of photometric redshifts. Including dispersion information may allow for mild internal self calibration of uncertainties in the true redshift distribution of observed SNeIa given their photometric redshifts. In the context of our models, this results in constraints on photometric redshift model parameters (see § 2) that are a factor of $\sim 2-5$ more constraining than the priors on these parameters from a spectroscopic sample of size $N_{\text{spec}} = 3000$. The realized level of improved calibration depends upon the details of both the model and the additional SNeIa calibration data that are available, but in all cases the luminosity distance test alone does not serve to calibrate the photometric redshift distribution.

Lastly, it is entirely possible that there will be evolution in the distribution of SNeIa intrinsic luminosities that significantly degrade the forecasts for dark energy constraints that

we present (see § 3). All approaches to SNeIa cosmology, even those that exploit the traditional luminosity distance test alone, rely upon some knowledge and/or assumptions about the intrinsic distribution of SNeIa luminosities to obtain cosmological constraints. In cases where the evolution of the spread in luminosities at fixed redshift is significant over the redshift range $0.2 \lesssim z \lesssim 0.8$, a photometric survey cannot use lensing to constrain dark energy directly. However, we have shown that such a survey can measure the evolution of the intrinsic SNeIa luminosity distribution at levels comparable to, or better than, a spectroscopic survey containing a few thousand SNeIa. This should aid the luminosity distance test by providing a better understanding of possible SNeIa evolution and demographics and, therefore, a better understanding of potential parameter biases and uncertainties.

As we have mentioned in the preceding paragraph, in examining a photometric SNeIa sample, it is necessary to consider uncertainties in the photometric redshift distribution. We have assumed that some calibration will be done with a spectroscopic sample of an unspecified size, N_{spec} . Figure 3 gives the expected area of the 95% ellipse in the w_0 - w_a plane, \mathcal{A} , as a function of N_{spec} . \mathcal{A} decreases rapidly with N_{spec} in all cases because increasing N_{spec} allows access to information over a broader range of observed redshifts and helps to break degeneracies in the w_0 - w_a plane. Figure 4 shows the constraints on the equation of state parameter at that redshift where the data best constrain it, the so-called pivot equation of state w_p , as a function of N_{spec} . This figure shows that the marginal improvement in $\sigma(w_p)$ with increasing N_{spec} decreases beyond $N_{\text{spec}} \sim \text{a few} \times 10^3$. This result is interesting because the upper limit on the achievable size of a spectroscopic sample is near $N_{\text{spec}} \sim 10^4$ and, moreover, with $N_{\text{spec}} \gtrsim 10^4$ constraints from the spectroscopic sample alone (which has miniscule redshift errors, $\sigma_z \sim 10^{-4}$) would begin to dominate over that achievable with a large, photometric sample even in the ideal limit where statistics, and not systematics, dominate the error budget. Both Fig. 3 and Fig. 4 illustrate that at fixed N_{spec} it is more fruitful to employ a spectroscopic calibration set weighted more toward high-redshift ($z \gtrsim 0.5$) SNeIa than the distribution of SNeIa from the imaging survey.

The previous paragraph closed with an allusion to systematic error, and indeed sources of systematic error are a major caveat to the present study. The main advantage of a photometric sample is its size and the additional statistical leverage that come with a large sample size. However, once systematic errors dominate the error budget, it is no longer possible to take advantage of this benefit. What is more, a photometric survey places emphasis on many potential sources of systematic error. We have accounted for some of these complications. For example, we have allowed for consistent determination of the photometric redshift distribution and for variation of the average SNeIa luminosity and intrinsic dispersion, including mild evolution. This is indicative that our results will be somewhat robust to evolution in the intrinsic SNeIa population (e.g. Hamuy et al. 1995; Howell 2001; Sullivan et al. 2006; Howell et al. 2007; Sarkar et al. 2008a). Other sources of systematic error are likely to be important. In fact, the SNAP collaboration, which aims to observe and exploit a spectroscopically-observed SNeIa sample from space, has assumed a fundamental limit in the ability to calibrate supernovae to within $\delta\mu \sim 0.02$ mag over a redshift difference of $\delta z \sim 0.1$ to specify their survey (e.g. Kim et al. 2004). Yet it remains to be seen whether such a systematic limit will

be realized, and it is possible that it may be higher or lower. Further, without spectroscopy, not only are redshifts uncertain, but supernovae type identification, extinction and K-corrections, and standard candle calibration all become more difficult (e.g. Pinto et al. 2004; Prieto et al. 2006). We have not explicitly accounted for any of these, largely because systematic levels are uncertain and modeling them is both complex and dependent upon survey strategy. These complications place a detailed treatment of systematics beyond the scope of our study (the studies by the DETF, as well as those of Zhan et al. 2008 and Hannestad et al. 2008 neglected a detailed treatment of systematics as well). If the assumed SNAP systematics floor is realized, our forecasts for dark energy equation of state constraints increase by a factor of ~ 3 , significantly reducing the additional cosmological information that may be extracted from the photometric sample of SNeIa.

As described in § 2, the calculations we have performed to estimate the additional information contained in the variety of SNeIa distance moduli at a fixed redshift are greatly simplified. Our idealization may lead to an over-estimate of the constraining power of SNeIa. However, we have also neglected some potentially-available information. In particular, the distribution of lensing magnifications is highly non-Gaussian (Schneider & Wagoner 1987; Sasaki 1987; Wambsganss et al. 1997; Munshi & Jain 2000; Wang et al. 2002) and we have neglected any information beyond the dispersion because including the full information is computationally-intensive and current theoretical estimates of the magnification distribution are inadequate for our application. The left panel of Figure 5 shows the non-Gaussianity of the lensing distribution at a fixed redshift $z = 0.8$ using the fitting formula of Wang et al. (2002). The right panel of Figure 5 shows the distribution of distance moduli in a bin of width $\delta z = 0.03$ centered at redshift $z = 0.8$. In our fiducial model, the bin contains roughly $n \approx 19,000$ SNeIa and Fig. 5 demonstrates that the non-Gaussianity of the lensing distribution would be detectable even by examining the distribution of distance moduli in this single bin. For the realization shown, the non-Gaussianity of the lensing distribution is detectable at slightly more than $\sim 2\sigma$ from this bin alone. This strongly suggests that the lensing deviation from Gaussianity may be detectable in a complete analysis of a future photometric survey, where the full shape of the magnification distribution would be utilized and where all supernovae could be considered (which requires better predictions). This is important for two reasons. First, the unique distribution of fluxes induced by lensing may aid in distinguishing the gravitational lensing effect from other additional sources of dispersion and from evolution in the intrinsic properties of SNeIa. Second, to the degree that this non-Gaussianity can be detected, it will bring additional information to bear and improve dark energy constraints.

To conclude, a future imaging survey that scans a large fraction of the sky rapidly will enable the discovery of $\sim 10^5 - 10^6$ SNeIa. The survey of the LSST is the canonical example of such an endeavor. The number of SNeIa with light curves of sufficient quality to be used for cosmology depend upon specific survey strategies; however, such a SNeIa survey may be able to constrain dark energy properties using both the traditional luminosity distance test and the spread of supernovae apparent brightnesses as a function of photometric redshift. Unfortunately, current theoretical treatments of gravitational lensing, in particular estimates of the magnification distribution, are not reliable enough to analyze any such data set. In the coming years, it will be necessary to

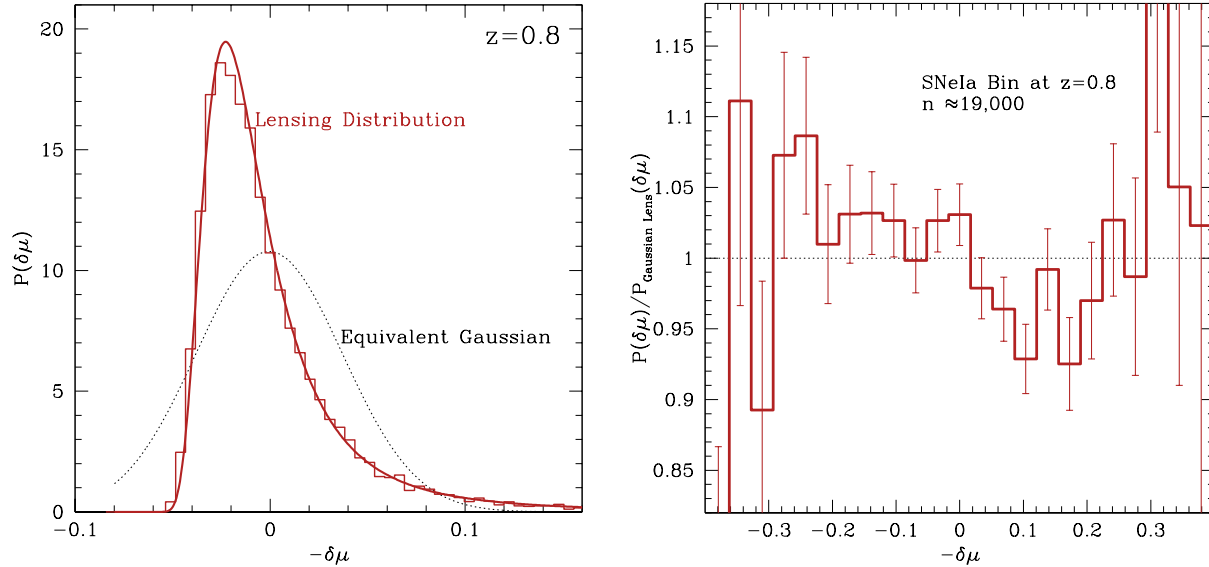


FIG. 5.— The non-Gaussianity of the lensing distribution. Both panels show the distribution of the shift in distance modulus $\delta\mu$ of SNIa. The *left* panel is illustrative. The *solid, smooth* curve shows the distribution of distance moduli for sources at redshift $z = 0.8$ due only to lensing. This result was computed using the fitting formula of Wang et al. (2002). We display this quantity at relatively high redshifts only because the formula of Wang et al. (2002) is no longer internally self-consistent below $z \sim 0.6$. The *dotted* curve shows a Gaussian distribution with the same mean and dispersion as the lensing distribution. The Gaussian distribution is truncated at the minimum magnification, corresponding to a maximum shift in distance modulus $\delta\mu_{\max}$. The distribution of distance modulus shifts from a random realization of 19,000 SNIa at $z = 0.8$. The *right* panel shows something closer to what would be seen in any observed set of SNIa. In this panel, we show the distribution of distance moduli (relative to the mean) for a random sample of SNIa in a bin of width $\delta z = 0.03$ at $z = 0.8$. The sample consists of 19,000 SNIa, which is roughly the number of SNIa expected in such a bin according to our fiducial model described in § 2. In this case, the distribution includes the intrinsic dispersion, the dispersion caused by poorly-controlled photometric redshifts, and the lensing distribution. For clarity, the probability distribution is plotted relative to the same distribution under the assumption of the lensing contribution is a Gaussian, $P_{\text{Gaussian Lens}}(\delta\mu)$. The error bars reflect the statistical error on $P(\delta\mu)$ from a sample of this size and portray of the detectability of the unique shape induced by lensing in the absence of significant errors.

refine these estimates, including potential theoretical uncertainties (Huterer & Takada 2005; Zhan & Knox 2004; White 2004; Rudd et al. 2008). In the end, the utility of such a sample to constrain dark energy is subject to limitations of systematic error and SNIa evolution. However, if observational systematics or SNIa evolution prove to be limiting, such a large photometric survey will provide useful information about these issues. In either case, an LSST-like imaging survey will revolutionize SNIa cosmology.

We would like to thank Lloyd Braun, David Cinabro, Sour-

ish Dutta, Scott Dodelson, Dragan Huterer, Arthur Kosowsky, Jeff Newman, Alberto Vallinotto, and Michael Wood-Vasey for useful discussions and email exchanges during the course of this work. ARZ is supported by the University of Pittsburgh and by the National Science Foundation through grant NSF AST 0806367. ARZ thanks the Michigan Center for Theoretical Physics at the University of Michigan for hospitality and support while some of this work was performed. SB is funded by a Mellon Predoctoral Fellowship at the University of Pittsburgh. This research made use of the National Aeronautics and Space Administration Astrophysics Data System.

REFERENCES

- Albrecht, A., Bernstein, G., Cahn, R., Freedman, W. L., Hewitt, J., Hu, W., Huth, J., Kamionkowski, M., Kolb, E. W., Knox, L., Mather, J. C., Stagg, S., & Suntzeff, N. B. 2006, (astro-ph/0609591)
- Aldering, G., Adam, G., Antilogus, P., Astier, P., Bacon, R., Bongard, S., Bonnaud, C., Copin, Y., Hardin, D., Henault, F., Howell, D. A., Lemonnier, J.-P., Levy, J.-M., Loken, S. C., Nugent, P. E., Pain, R., Pecontal, A., Pecontal, E., Perlmutter, S., Quimby, R. M., Schahmanche, K., Smadja, G., & Wood-Vasey, W. M. 2002, in Presented at the Society of Photo-Optical Instrumentation Engineers (SPIE) Conference, Vol. 4836, Survey and Other Telescope Technologies and Discoveries. Edited by Tyson, J. Anthony; Wolff, Sidney. Proceedings of the SPIE, Volume 4836, pp. 61-72 (2002), ed. J. A. Tyson & S. Wolff, 61–72
- Astier, P., Guy, J., Regnault, N., Pain, R., Aubourg, E., Balam, D., Basa, S., Carlberg, R. G., Fabbro, S., Fouchez, D., Hook, I. M., Howell, D. A., Lafoux, H., Neill, J. D., Palanque-Delabrouille, N., Perrett, K., Pritchet, C. J., Rich, J., Sullivan, M., Taillet, R., Aldering, G., Antilogus, P., Arsenijevic, V., Balland, C., Baumont, S., Bronder, J., Courtois, H., Ellis, R. S., Filiol, M., Gonçalves, A. C., Goobar, A., Guide, D., Hardin, D., Lussat, V., Lidman, C., McMahon, R., Mouchet, M., Mourao, A., Perlmutter, S., Ripoche, P., Tao, C., & Walton, N. 2006, A&A, 447, 31
- Barber, A. J. 2000, MNRAS, 318, 195
- Bernardeau, F., van Waerbeke, L., & Mellier, Y. 1997, A&A, 322, 1
- Christensen, N. & Meyer, R. 2001, Phys. Rev. D, 64, 022001
- Christensen, N., Meyer, R., Knox, L., & Luey, B. 2001, Classical and Quantum Gravity, 18, 2677
- Cooray, A., Holz, D. E., & Huterer, D. 2006, ApJ, 637, L77
- Copin, Y., Blanc, N., Bongard, S., Gangler, E., Saugé, L., Smadja, G., Antilogus, P., Garavini, G., Gilles, S., Pain, R., Aldering, G., Bailey, S., Lee, B. C., Loken, S., Nugent, P., Perlmutter, S., Scalzo, R., Thomas, R. C., Wang, L., Weaver, B. A., Pécontal, E., Kessler, R., Baltay, C., Rabinowitz, D., & Bauer, A. 2006, New Astronomy Review, 50, 436
- Dodelson, S. & Vallinotto, A. 2006, Phys. Rev. D, 74, 063515
- Guy, J., Astier, P., Baumont, S., Hardin, D., Pain, R., Regnault, N., Basa, S., Carlberg, R. G., Conley, A., Fabbro, S., Fouchez, D., Hook, I. M., Howell, D. A., Perrett, K., Pritchet, C. J., Rich, J., Sullivan, M., Antilogus, P., Aubourg, E., Bazin, G., Bronder, J., Filiol, M., Palanque-Delabrouille, N., Ripoche, P., & Ruhlmann-Kleider, V. 2007, A&A, 466, 11
- Hagan, B., Ma, C.-P., & Kravtsov, A. V. 2005, ApJ, 633, 537
- Hamuy, M., Phillips, M. M., Maza, J., Suntzeff, N. B., Schommer, R. A., & Aviles, R. 1995, AJ, 109, 1

- Hannestad, S., Haugbølle, T., & Thomsen, B. 2008, *Journal of Cosmology and Astro-Particle Physics*, 2, 22
- Holz, D. E. 1998, *ApJ*, 506, L1
- Holz, D. E. & Linder, E. V. 2005, *ApJ*, 631, 678
- Howell, D. A. 2001, *ApJ*, 554, L193
- Howell, D. A., Sullivan, M., Conley, A., & Carlberg, R. 2007, *ApJ*, 667, L37
- Hu, W. & Jain, B. 2004, *Phys. Rev. D*, 70, 043009
- Huterer, D., Kim, A., Krauss, L. M., & Broderick, T. 2004, *ApJ*, 615, 595
- Huterer, D. & Takada, M. 2005, *Astroparticle Physics*, 23, 369
- Huterer, D. & Turner, M. S. 2001, *Phys. Rev. D*, 64, 123527
- Jha, S., Riess, A. G., & Kirshner, R. P. 2007, *ApJ*, 659, 122
- Jungman, G., Kamionkowski, M., Kosowsky, A., & Spergel, D. N. 1996, *Phys. Rev. D*, 54, 1332
- Kantowski, R., Vaughan, T., & Branch, D. 1995, *ApJ*, 447, 35
- Kim, A. G., Linder, E. V., Miquel, R., & Mostek, N. 2004, *MNRAS*, 347, 909
- Knox, L., Christensen, N., & Skordis, C. 2001, *ApJ*, 563, L95
- Komatsu, E., Dunkley, J., Nolta, M. R., Bennett, C. L., Gold, B., Hinshaw, G., Jarosik, N., Larson, D., Limon, M., Page, L., Spergel, D. N., Halpern, M., Hill, R. S., Kogut, A., Meyer, S. S., Tucker, G. S., Weiland, J. L., Wollack, E., & Wright, E. L. 2008, *ApJS Submitted*, ArXiv e-prints, 803
- Kosowsky, A., Milosavljevic, M., & Jimenez, R. 2002, *Phys. Rev. D*, 66, 063007
- Linder, E. V., Wagoner, R. V., & Schneider, P. 1988, *ApJ*, 324, 786
- Ma, Z., Hu, W., & Huterer, D. 2006, *ApJ*, 636, 21
- Mannucci, F., Della Valle, M., & Panagia, N. 2006, *MNRAS*, 370, 773
- Metcalf, R. B. 1999, *MNRAS*, 305, 746
- Munshi, D. & Jain, B. 2000, *MNRAS*, 318, 109
- Phillips, M. M. 1993, *ApJ*, 413, L105
- Pinto, P. A., Smith, C. R., & Garnavich, P. M. 2004, *BAAS*, 36, 1530
- Prieto, J. L., Rest, A., & Suntzeff, N. B. 2006, *ApJ*, 647, 501
- Riess, A. G., Press, W. H., & Kirshner, R. P. 1996, *ApJ*, 473, 88
- Riess, A. G., Strolger, L.-G., Casertano, S., Ferguson, H. C., Mobasher, B., Gold, B., Challis, P. J., Filippenko, A. V., Jha, S., Li, W., Tonry, J., Foley, R., Kirshner, R. P., Dickinson, M., MacDonald, E., Eisenstein, D., Livio, M., Younger, J., Xu, C., Dahlsen, T., & Stern, D. 2007, *ApJ*, 659, 98
- Rudd, D. H., Zentner, A. R., & Kravtsov, A. V. 2008, *ApJ*, 672, 19
- Sarkar, D., Amblard, A., Cooray, A., & Holz, D. E. 2008a, ArXiv e-prints, 806
- Sarkar, D., Amblard, A., Holz, D. E., & Cooray, A. 2008b, *ApJ*, 678, 1
- Sasaki, M. 1987, *MNRAS*, 228, 653
- Schneider, P. & Wagoner, R. V. 1987, *ApJ*, 314, 154
- Seljak, U. 1997, *ApJ*, 482, 6
- Smith, R. E., Peacock, J. A., Jenkins, A., White, S. D. M., Frenk, C. S., Pearce, F. R., Thomas, P. A., Efstathiou, G., & Couchman, H. M. P. 2003, *MNRAS*, 341, 1311
- Sullivan, M., Le Borgne, D., Pritchet, C. J., Hodsman, A., Neill, J. D., Howell, D. A., Carlberg, R. G., Astier, P., Aubourg, E., Balam, D., Basa, S., Conley, A., Fabbro, S., Fouchez, D., Guy, J., Hook, I., Pain, R., Palanque-Delabrouille, N., Perrett, K., Regnault, N., Rich, J., Taillet, R., Baumont, S., Bronder, J., Ellis, R. S., Filoli, M., Lusset, V., Perlmutter, S., Riposte, P., & Tao, C. 2006, *ApJ*, 648, 868
- Tegmark, M., Taylor, A. N., & Heavens, A. F. 1997, *ApJ*, 480, 22
- Valageas, P. 2000, *A&A*, 356, 771
- Wambsganss, J., Cen, R., Xu, G., & Ostriker, J. P. 1997, *ApJ*, 475, L81+
- Wang, Y. 1999, *ApJ*, 525, 651
- Wang, Y., Holz, D. E., & Munshi, D. 2002, *ApJ*, 572, L15
- Wang, Y., Narayan, G., & Wood-Vasey, M. 2007, *MNRAS*, 382, 377
- White, M. 2004, *Astroparticle Physics*, 22, 211
- Wood-Vasey, W. M., Miknaitis, G., Stubbs, C. W., Jha, S., Riess, A. G., Garnavich, P. M., Kirshner, R. P., Aguilera, C., Becker, A. C., Blackman, J. W., Blondin, S., Challis, P., Clocchiatti, A., Conley, A., Covarrubias, R., Davis, T. M., Filippenko, A. V., Foley, R. J., Garg, A., Hicken, M., Krisciunas, K., Leibundgut, B., Li, W., Matheson, T., Miceli, A., Narayan, G., Pignata, G., Prieto, J. L., Rest, A., Salvo, M. E., Schmidt, B. P., Smith, R. C., Sollerman, J., Spyromilio, J., Tonry, J. L., Suntzeff, N. B., & Zenteno, A. 2007, *ApJ*, 666, 694
- Zentner, A. R., Rudd, D. H., & Hu, W. 2008, *Phys. Rev. D*, 77, 043507
- Zhan, H. & Knox, L. 2004, *ApJ*, 616, L75
- Zhan, H., Wang, L., Pinto, P., & Tyson, J. A. 2008, *ApJ*, 675, L1
- Zhang, P. & Chen, X. 2008, *Phys. Rev. D*, 78, 023006